©ESO 2024

A Cohesive Deep Drilling Field Strategy for LSST Cosmology

Philippe Gris[1], Humna Awan[2], Matthew R. Becker[3], Huan Lin[4], Eric Gawiser[5], Saurabh W. Jha[5], and
the LSST Dark Energy Science Collaboration

[1] Laboratoire de Physique de Clermont Auvergne, IN2P3/CNRS, F-63000 Clermont-Ferrand, France
[2] Leinweber Center for Theoretical Physics, Department of Physics, University of Michigan, Ann Arbor, MI 48109, USA
[3] High Energy Physics Division, Argonne National Laboratory, Lemont, IL 60439, USA
[4] Fermi National Accelerator Laboratory, USA
[5] Department of Physics and Astronomy, Rutgers, The State University of New Jersey, Piscataway, NJ 08854, USA

May 20, 2024

ABSTRACT

The Vera C. Rubin Observatory Legacy Survey of Space and Time (LSST) will image billions of astronomical objects in the wide-fast-deep primary survey and in a set of minisurveys including intensive observations of a group of deep drilling fields (DDFs). The DDFs are a critical piece of three key aspects of the LSST Dark Energy Science Collaboration (DESC) cosmological measurements: they provide a required calibration for photometric redshifts and weak gravitational lensing measurements and they directly contribute to cosmological constraints from the most distant type Ia supernovae. We present a set of cohesive DDF strategies fulfilling science requirements relevant to DESC and following the guidelines of the Survey Cadence Optimization Committee. We propose a method to estimate the observing strategy parameters and we perform simulations of the corresponding surveys. We define a set of metrics for each of the science case to assess the performance of the proposed observing strategies. We show that the most promising results are achieved with deep rolling surveys characterized by two sets of fields: ultradeep fields ($z \lesssim 1.1$) observed at a high cadence with a large number of visits over a limited number of seasons; deep fields ($z \lesssim 0.7$), observed with a cadence of ∼3 nights for ten years. These encouraging results should be confirmed with realistic simulations using the LSST scheduler. A DDF budget of ∼8.5% is required to design observing strategies satisfying all the cosmological requirements. A lower DDF budget lead to surveys that either do not fulfill photo-z/WL requirements or are not optimal for SNe Ia cosmology.

1. Introduction

The Vera C. Rubin Observatory Legacy Survey of Space and Time (LSST; Ivezić et al. (2019)) will image billions of objects in six bands for ten years. The observing time will be shared between the wide-fast-deep (WFD) primary survey, which will cover half of the sky (∼20,000 deg²), and a set of minisurveys, including intensive observation of a set of deep drilling fields (DDFs). In the WFD survey, fields are observed with a similar cadence and pattern, the cadence beeing defined as the median internight gap in any filter (high cadences correspond to small internight gaps). The DDF mini-survey is characterized by a high cadence of observation, a high number of visits per observing night, and a limited survey area (60-70 deg²).

The DDF mini-survey is vital for achieving the core science the LSST Dark Energy Science Collaboration (DESC; Abate (2012)) and it has three main drivers: cosmology, calibration of primary systematic uncertainties for several cosmological measurements, and synergy with other surveys. DDFs are essential for DESC to reach its Stage IV dark energy goals, that is to multiply by ∼ 10 the Figure of Merit (FoM) of stage II surveys (Albrecht et al. 2006).

DESC has long emphasized the importance of the observing strategy for science probes (or key input to science probes) used to measure cosmological parameters (dark energy equation of state) with high accuracy. Many studies have already been achieved (Awan et al. (2016), Lochner et al. (2018), Scolnic et al. (2018), Almoubayyed et al.

(2020), Lochner et al. (2021a), Lochner et al. (2021b), Gris et al. (2023), Alves et al. (2023)) and the work presented in this paper is a continuation of many years of efforts aiming to define the optimal observing strategy to accomplish the scientific objectives of the Rubin Observatory. In the following we focus on the design of the DDF mini-survey which is critical for three DESC cosmological measurements: photometric redshifts, weak gravitational lensing, and Type Ia Supernovae, as outlined in the text that follows.

LSST is expected to provide useful shape measurements in six-band photometry for about 4 billion of galaxies (Abell et al. 2009). It is infeasible to measure redshifts via spectroscopy for such a large number of galaxies, extending to faint magnitudes, and widely distributed. LSST will thus primarily rely on photometric redshifts (photo-z) based only on imaging information. A key ingredient for all LSST photometric measurement techniques is a training set of galaxies with highly reliable redshifts. DDFs in LSST lead to much deeper coadded observations with respect to the WFD survey and overlap with deep spectroscopic redshifts (Le Fèvre et al. 2013) and deep photometric redshift samples (Weaver et al. 2022). These samples are essential for redshift calibration purposes.

Weak gravitational lensing (WL), the deflection of light from distant massive structures, is currently one of the most promising probes to constrain the growth of the cosmic structure and unveil the nature of dark energy (Mandelbaum (2018) and references therein). The LSST survey will dramatically increase the statistical power of WL measure-

ments by observing billions of galaxies. Two key parameters are to be extracted from LSST data: the shear from galaxy shapes, and the photometric redshift estimates. Shear signals are to be measured with systematic errors lower than $\sim 10^{-3}$ to minimize the degradation in cosmological parameter accuracies (Huterer et al. 2006). The shear calibration bias, one of the largest systematic error sources, may be reduced using self-calibration techniques such as META-CALIBRATION (Huff & Mandelbaum (2017), Sheldon & Huff (2017)) where real images are used to simulate the effect of a known shear. Using the METACALIBRATION method in images collected in the WFD survey would lead to a $\sim 20\%$ loss of precision in the statistical shear measurements (Zhang et al. 2023). Reducing this loss (pixel noise) to $\lesssim 5\%$ in METACALIBRATION estimators of weak lensing signals requires using the DDFs and the DEEP-FIELD META-CALIBRATION technique (Zhang et al. 2023).

Type Ia Supernovae (SNe Ia) are the results of powerful and luminous explosions of white dwarfs. SNe Ia can be considered as standardizable candles to estimate distances used to measure cosmological parameters (equation of state of dark energy) in a Hubble diagram (Betoule et al. (2014), Brout et al. (2022)). Cosmological distances are estimated from SNe Ia parameters extracted from photometric observations (SNe Ia light curves) generated by the observing strategy. Hence measuring cosmological parameters with a high accuracy requires optimizing the observing strategy to collect high quality light curves (in terms of sampling and signal-to-noise ratio). LSST will observe a large number of SNe Ia at low redshifts ($z \lesssim 0.4$) in the WFD survey (Lochner et al. 2021a). Measuring w_0 and w_a parameters of the equation of state of dark energy requires to observe (necessary condition) a large sample of SNe Ia at higher redshifts (up to $z \sim 1.1$) and this is only feasible with DDFs (Gris et al. 2023). DDFs are thus critical if LSST is expected to address dark energy physics and cosmology with SNe Ia.

The purpose of this paper is to design a DESC cohesive DDF program that would fulfill calibration requirements (photo-z and WL) and cosmological constraints (SNe Ia) whilst meeting the Survey Cadence Optimization Committee (SCOC; Bianco et al. (2021)) phase 2 guidelines (The Rubin Observatory Survey Cadence Optimization Committee 2022). This article is divided in four sections. The design requirements of the survey are detailed in Section 2 with a summary of the SCOC phase 2 recommendations (subsection 2.1) and a detailed explanation of the requirements from cosmology measurements (subsection 2.2). A set of metrics to assess observing strategy and to quantify to which extent science requirements are met are defined in Section 3. These metrics are based on statistical optimization and do not include systematic uncertainties. A proposed cohesive DDF strategy is presented in Section 4 along with the methodology used to define observing strategy parameters leading to DDF surveys compliant with science requirements. These strategies are simulated and assessed in Section 5 using the metrics defined in Section 3.

2. Design requirements

2.1. SCOC phase 2 recommendations

The SCOC phase 2 recommendations are summarized in The Rubin Observatory Survey Cadence Optimization Committee (2022). The main points concerning the Deep Drilling program are:

- budget (i.e. fraction of visits corresponding to DD observations) in the range 5%-7%;
- 5 DDFs to be observed for ten years. 4 fields (COSMOS, CDF-S, ELAIS-S1, XMM-LSS) were selected in 2012 (https://ls.st/bki). A 5th field, the Euclid Deep Field South (EDFS), is added, with a footprint roughly twice as large as the extent of the other DDFs. This field will be observed at half the exposure time of the other DDFs;
- COSMOS should be prioritized with additionnal survey time to reach 10-year DDF depth within the first three years of LSST. COSMOS will continue to be observed thereafter at the same rate as other DDFs. There are two main reasons for starting the DDF observations early: the DESC DDF photo-z calibration will be improved by the earlier information; at least one DDF should be completed early for low-surface-brightness science and calibration purposes (Galaxies Science Collaboration).

Two critical aspects are still to be defined, the cadence of observation, and the filter allocation (i.e. the number of visits per band and per observing night). The goal of this paper is to propose a set of values for those parameters whilst taking into account the recommendations of the SCOC. The resulting observing strategies should also meet Photo-z, Weak Lensing, and SNe Ia requirements detailed in the following.

2.2. Requirements from cosmological measurements

2.2.1. Photo-z

Photometric redshifts in LSST are estimated from the Spectral Energy Density (SED) of distant galaxies, integrated over 6 bands. The type and redshift measured from the flux observed in multi-band is frequently not uniquely defined: two different rest-frame SEDs observed at two different redshifts can be difficult to distinguish. The type/redshift degeneracy is one of the main causes of uncertainty in photometric redshift calibration.

It may be possible to break degeneracies by combining wide-field, multi-band measurements with accurate redshift galaxies. In deep-fields, precise photometry of multi-band flux can be used to group galaxies into fine-grained set of phenotypes (Sánchez & Bernstein 2018), which are types of galaxy based on observed flux rather than on rest-frame properties. The multi-band deep fields provide greater opportunities to assess the impact of selection effects.The set of galaxy photometry and a set of galaxies with confidently known z (obtained using many-band photometry observations or spectroscopy) can be used as input to a photometric method such as SOMPZ which is based upon the self-organizing map algorithm (Buchs et al. (2019), Myles et al. (2021)).

The coadded DDFs go much deeper than those of the WFD area and overlap deep spectroscopic redshift surveys (e.g., VIMOS VLT Deep Survey (VVDS), Euclid Complete Calibration of the Color-Redshift Relation (C3R2),

Le Fèvre et al. 2013; Stanford et al. 2021), deep photometric redshift samples (COSMOS2020, Weaver et al. 2022), Spitzer/IRAC data (SERVS, Mauduit et al. 2012), and deep NIR catalogs (UltraVISTA, McCracken, H. J. et al. 2012; VIDEO, Jarvis et al. 2012). The deep *ugrizy* photometry from the DDF overlaps of these deep spec-z and photo-*z* samples are essential for enabling calibrations of the galaxy redshift distributions needed for LSST science. We therefore define photo-*z* requirements for the *ugrizy* depths in the DDF areas based on redshift calibration considerations, in particular in the following two cases.

Year 1 (Y1): We first set requirements at the end of LSST Y1, in order to enable the use of the C3R2 and VVDS deep spectroscopic redshift samples for redshift calibrations. We define the requirements based on measuring good photometry for 95% of the C3R2 and VVDS samples, with good photometry defined as measuring 2-arcsec diameter aperture magnitudes at 10-σ for *griz* and 5-σ for *uy*. We measure these magnitude limits using the magnitude histograms of C3R2 and VVDS galaxy redshift samples overlapping the DES Year 3 Deep Field photometry catalog (Hartley et al. 2021). These aperture magnitude limits are translated to 5-σ point source limits, assuming a Gaussian point spread function (PSF) and typical seeing FWHM of 0.8 arcsec, resulting in LSST Y1 5-σ point source depths for the *ugrizy* bands (Table 1). These depths are meant to apply to the 5th percentile values of the Coaddm5Metric (Equation 4) evaluated for healpixels within a radius of 1.6 degrees from the center of each DDF. The 5th percentile depth accounts for significant spatial non-uniformities in depth in early years and is a compromise between minimum (too stringent) and median (too relaxed) values.

Table 1: PZ requirements. 5-σ point source depths for year 1 and for year 10. Depths for year 2-9 will be scaled from year 10 requirements.

band	Y1	Y10
u	26.7	27.8
g	27.0	28.1
r	26.2	27.8
i	25.8	27.6
z	25.6	27.2
y	24.7	26.5

Years 2-10 (Y10): We set requirements scaling with time so that at the end of LSST Y10, the ugrizy magnitude limits match those of the COSMOS2020 imaging. The flux limit scales with the square root of the exposure time and decreases from Y1 to Y10. This would enable the deep DDF photometry, apart from their overlaps with external spec-z and photo-*z* samples, to be used for redshift calibration, e.g., via self organizing map (SOM) methods as used in the Dark Energy Survey (Myles et al. 2021). We translate the quoted COSMOS2020 3-σ 2-arcsec diameter aperture magnitude depths (Weaver et al. 2022) to LSST 5-σ point source depths for the *ugrizy* bands (Table 1).

2.2.2. Weak Lensing

The weak lensing requirements are driven by two primary uses of the DDFs. First, DDF imaging that overlaps or will overlap with high-resolution space-based imaging (e.g.,

COSMOS or Euclid) is essential for generating realistic simulations for testing the calibration of weak lensing shape estimation methods (e.g., MacCrann et al. 2022). Second, the DDFs are used to calibrate certain weak lensing shear estimators, including the Bayesian Fourier Domain (BFD) technique (Bernstein & Armstrong 2014; Bernstein et al. 2016) and the deep-field metacalibration technique (Zhang et al. 2023).

The requirements for both of these use cases can be phrased in terms of the relative number of visits between the DDFs and the WFD. First, for the image simulation use case, previous studies have found that image simulations for weak lensing shear calibration need to have galaxies down to ≈1.5 magnitudes fainter than the limiting magnitude being calibrated in order to limit calibration errors to $\lesssim$ 0.1% (Hoekstra et al. 2015, 2017). Assuming the sources are background-dominated, this requirement implies that the DDFs used to derive input sources for WL shear calibration simulations have $\gtrsim$ 16× as many visits as the WFD. This number is derived from Equation 4 below, assuming a target increased coadded depth of 1.5 magnitudes. Importantly, this requirement would only apply to regions with imaging that overlaps with a space-based survey. Further, a joint analysis of the ground- and space-based imaging will greatly benefit from both this increased depth and from the much smaller effective PSF of the space-based data. At minimum, this would include COSMOS data but might also include Euclid data as well.

Second, the primary requirement for BFD and deep-field metacalibration is that the pixel noise in the DDF coadd images be sufficiently smaller than the typical pixel noise in WFD coadd images. Working in the background-dominated limit and assuming a simple mean coaddition strategy, the relative pixel noise in the mean coadd image between the DDF and WFD data will decrease as the square root of the ratio of the number of DDF to WFD visits. Both techniques require this ratio to be $\gtrsim$ 10 for essentially the same reason: limiting the DDF contribution to the variance in the weak lensing shape estimator to $\lesssim$ 10%.

We finally end up with two WL requirements related to the ratio of the number of DDF visits to the number of WFD visits $r = \frac{N_v^{DDF}}{N_v^{WFD}}$: $r \gtrsim 16$ (WL shear calibration for e.g. COSMOS) and $r \gtrsim 10$ (pixel noise). We thus assume a requirement of at least 10× as many visits in the DDFs as the WFD. We do not impose to have $r \gtrsim 16$ for e.g. COSMOS but we will check whether this requirement is fulfilled in the strategies proposed in this paper.

The WL requirements are summarized in Table 2. We have specified the required number of visits for Y1 and Y10. However, note that the above WL requirements must be satisfied at any data release in the survey that we wish to use for cosmological analysis. These data releases will include Y1 and Y10, and will also include intermediate data releases e.g., Y4 and Y7.

2.2.3. SNe Ia

The estimation of the cosmological parameters with SNe Ia is achieved by fitting the distance modulus (indirect measure of distance using brightness) versus redshift relation. The distance modulus depends on SNe Ia parameters which are estimated from photometric observations (light curve) emanating from the survey (observing strat-

Table 2: Number of visits (per band) required to fulfill photo-z and WL requirements.

band	m_5^{single}	photo-z requirements N$_{\text{visit}}$		WL requirements N$_{\text{visit}}$		WL+photo-z (WZ) requirements N$_{\text{visit}}$	
		season 1	season 2-10	season 1	season 2-10	season 1	season 2-10
u	23.53	343	2601	48	432	343	2601
g	24.23	165	1252	72	648	165	1252
r	23.70	100	1905	184	1656	184	1905
i	23.33	94	2592	184	1656	184	2592
z	22.95	131	2493	152	1368	152	2493
y	22.17	105	2884	160	1440	160	2884

egy). Measuring cosmological parameters with a high degree of accuracy requires minimizing SNe Ia parameter errors, that is to maximize the light curve signal-to-noise ratio (SNR) per band b, SNR^b, defined by:

$$\text{SNR}^b = \sqrt{\sum_{i=1}^{n^b} \left(\frac{f_i^b}{\sigma_i^b} \right)^2} \qquad (1)$$

where f^b, and σ^b are the fluxes and flux uncertainties. The sum runs over observations within a time-window around the SN Ia luminosity peak MJD (see subsection 3.3). The main strategy parameters impacting SNR^b are the cadence of observation (SNR^b increases with an increase of the cadence) and the number of visits per observing night and per band N$_{visits}^b$. The light curve flux errors σ_i^b decreases with an increase of N$_{visits}^b$. This can be explained as follows. In the background-dominated regime one has $\sigma_i^b \simeq \sigma_5^b$ where σ_5^b is equal by definition to

$$\sigma_5^b = \frac{f_5^b}{5} \qquad (2)$$

where f_5^b is the 5-σ flux related to the 5-σ magnitude m_5^b. The coadded 5-σ depth increases (and σ_i^b decreases) with the number of visits (see Equation 4). Nightly DDF coadded observations lead to an increase of SNR^b values which translates into a significant increase of well-observed SNe Ia at higher redshift.

The redshift distribution of the sample of well-measured SNe Ia is critical to measure dark energy parameters. The WFD survey will provide a low-z sample ($0.01 \gtrsim z \gtrsim 0.4 - 0.6$) which will be combined with a high-z ($0.3 \gtrsim z \gtrsim 1.1$) DDF SNe Ia sample necessary to measure (w_0, w_a) parameters with high accuracy (Gris et al. 2023). It is possible to quantify the depth of the survey using the redshift completeness z_{complete} (see the definition in Appendix A), a parameter correlated with SNR^b (Gris et al. 2023). Increasing z_{complete} leads to an increase of the number of well-sampled SNe Ia at higher redshifts and requires to boost SNR^b values with a survey strategy characterised by a high cadence of observation (1-2 nights), a large number of visits per observing night (typically more than hundred for a cadence of 1 night), and a filter allocation optimized to observe at higher redshifts (Table 3).

The DDF budget is limited to 5-7% (The Rubin Observatory Survey Cadence Optimization Committee 2022). It is thus impossible, according to the numbers in Table 3 to observe a full sample of SNe Ia up to high redshift completeness ($z_{\text{complete}} \gtrsim 0.75$) with a survey scanning 5

Table 3: Number of visits per observing night and filter allocation required to reach z_{complete} of 0.80, 0.75, and 0.70. The cadence of observation is of one night and the season length of 180 days. These results are extracted from Gris et al. (2023).

z_{complete}	N$_{\text{visit}}$/obs. night		budget
	total	$g/r/i/z/y$	per season
0.80	149	2/9/62/56/20	1.3%
0.75	108	2/9/44/38/15	0.9%
0.70	81	2/9/33/31/6	0.7%

fields for ten years. One way to maximize the number of SNe Ia at higher redshifts is then to define two types of DDFs: Deep Fields (DFs) with a redshift completeness lower than ~ 0.60; Ultra-Deep Fields (UDF) with observing strategy parameters corresponding to Table 3 for a limited number of seasons (typically between 2 to 4); UDFs are observed with the same strategy as DFs for the remaining seasons. Optimized scenarios include the observation of two UDFs for two ($z_{\text{complete}} \sim 0.80$), three ($z_{\text{complete}} \sim 0.75$), or four ($z_{\text{complete}} \sim 0.70$) seasons.

3. Metrics to assess observing strategies

3.1. Photo-z

Photo-z calibration requirements can be translated to 5-σ depth point source constraints (subsubsection 2.2.1). We define the photo-z metric as the (coadded per band) 5-σ depth difference between observing strategy observations and the requirements defined in Table 2:

$$\Delta m_5^b = m_5^{b,OS} - m_5^{b,PZ \ req.} \qquad (3)$$

where b is the band and $m_5^{b,OS}$ is the coadded 5-σ depth:

$$m_5^{b,OS} = 1.25 \log_{10} \sum_{i=1}^{N_v^b} (10^{0.8 \ m_5^{b,i}}) \qquad (4)$$

Equation 4 equates to adding signal-to-noise ratio for a background-limited object in quadrature and may be written as:

$$m_5^{b,OS} = 1.25 \log_{10} N_v^b + <m_5^{b,i}> + \Delta m_5^{b,i} \qquad (5)$$

where N_v^b is the number of visits in the b band and $<m_5^{b,i}>$ is the 5-σ depth mean value. $\Delta m_5^{b,i}$ depends on the standard deviation of the $m_5^{b,i}$ values. From the LSST simulation baseline_v3.0_10yrs we obtain $<\Delta m_5^{b,i}> \sim \mathcal{O}(0.01)$

for the COSMOS field. In this paper we have used $\Delta m_5^{b,i}=0$ since we have considered median observing conditions per season (Section 5).

Photo-z requirements are fulfilled if $\Delta m_5^b \geq 0$.

3.2. Weak Lensing

Following the WL requirements (subsubsection 2.2.2) we define the photo-z metric as:

$$r^{WL} = \frac{N_{visits}^{OS}}{N_{visits}^{WL\ req}} \tag{6}$$

where N_{visits}^{OS} is the number of visits (per band) of the proposed strategies and $N_{visits}^{WL\ req}$ the number of visits corresponding to WL requirements (Table 2). WL requirements are fulfilled if $r^{WL} \geq 1$.

3.3. SNe Ia

The metric used to assess the strategies proposed in this paper is based on the Dark Energy Task Force (DETF) Figure of merit (Albrecht et al. 2006). It is estimated from the result of a cosmological fit using SNe Ia and is defined as:

$$\text{Supernova Metric of Merit (SMoM)} = \frac{\pi}{A} \tag{7}$$

where A is the area of the confidence ellipse defined by:

$$A = \pi \Delta\chi^2 \sigma_{w_0} \sigma_{w_a} \sqrt{1 - \rho^2} \tag{8}$$

with $\Delta\chi^2 = 6.17$ (95.4% C.L. for 2 degrees of freedom). ρ is the correlation factor equal to $\text{Cov}(w_0, w_a)/(\sigma_{w_0}\sigma_{w_a})$. w_0 and w_a are the parameters of the Chevallier-Polarski-Linder (CPL) model of the dark energy equation of state (Chevallier & Polarski 2001; Linder 2003):

$$w = w_0 + w_a \frac{z}{1+z} \tag{9}$$

The cosmological parameters are estimated by minimizing:

$$-ln\mathcal{L} = \sum_{i=1}^{N_{SN}} \frac{(\mu_i - \mu_{th}(z_i, \Omega_m, w_0, w_a))^2}{\sigma_{\mu_i}^2 + \sigma_{int}^2} \tag{10}$$

where N_{SN} is the number of well-sampled SNe Ia (definition below), σ_μ the distance modulus error, and σ_{int} the intrinsic dispersion of SNe Ia ($\sigma_{int} \sim 0.12$ mag).

We simulate SNe Ia distance moduli using:

$$\mu_i(z_i) \sim \mathcal{N}(\mu_{th}(z_i, \Omega_m, w_0, w_a), \sigma^2 = \sigma_{\mu_i}^2 + \sigma_{int}^2) \tag{11}$$

Distance moduli errors, σ_{μ_i}, are estimated from SNe Ia simulations. We use the SALT3 model (Kenworthy et al. 2021) to simulate and fit SNe Ia light curves. In this model, the distance modulus, μ, is defined for each SN Ia by:

$$\mu = m_B + \alpha x_1 - \beta c - M \tag{12}$$

where $m_B = -2.5 \log_{10}(x_0) + 10.635$, where x_0 is the overall flux normalization, x_1 describes the width of the light curve, c is equal to a color offset (with respect to the average) at the date of peak brightness in B-band, $c = (B - V)_{MAX} - <B - V>$. For each SN Ia, m_B, x_1, c parameters are estimated from a fit of a SN Ia model to

the measurements of a multicolor light curve. α, β and M are global parameters estimated from the data. M is the absolute magnitude in rest-frame B-band for a median SN Ia with $(x_1,c) = (0.0, 0.0)$. α and β are global nuisance parameters quantifying the correlation between brightness with x_1 and c, respectively. The three parameters α, β, M are usually fitted along with cosmological parameters by minimizing Equation 10. In this study we set α, β, and M to their simulated values so as to fit only cosmological parameters.

In the SALT3 model a SNe Ia is described by five parameters: x_0, x_1, c, z (redshift), and T_0 (time of maximum luminosity). For each of the proposed strategies we have simulated a sample of SNe Ia corresponding to 30 times the number of expected SNe Ia (we use the rate Hounsell et al. (2018)) in the full redshift range [0.01,1.1]. Concerning the (x_1,c) distribution of SNe Ia, we use the G10 intrinsic scatter model (Scolnic & Kessler 2016) where (x_1,c) distributions are described by asymmetric gaussian distributions with three parameters. We choose random T_0 values spanning over the season duration of a group of observations.

We use SNCosmo (Barbary et al. 2016), a Python library synthesizing SN spectra and photometry from SN models, to simulate and fit SNe Ia light curves using the SALT3 model. The telescope throughput curves (detector, lenses, mirrors, filters) used to estimated SNe Ia fluxes are consistent with the LSST simulations considered in this paper (v1.5 of https://github.com/lsst/throughputs). The set of well-sampled SNe Ia used to estimate SMoM is composed of SNe Ia fulfilling the requirements detailed in Table 4.

Table 4: Selection criteria leading to a sample of well-sampled SNe Ia based on the available phases p=$\frac{t-T_0}{1+z}$ of photometric observations at time t. (a) and (b) correspond to Guy et al. (2010) and Betoule et al. (2014), respectively.

Selection	Rationale
light curve (LC)	
$N_{epochs}(p \leq -10) \geq 1$	low phase LC
$N_{epochs}(p \geq +20) \geq 1$	high phase LC
$N_{epochs}(-10 \leq p \leq 35) \geq 4$	SN parameters (a)
$N_{epochs}(-10 \leq p \leq 5) \geq 1$	SN parameters (a)
$N_{epochs}(+5 \leq p \leq 20) \geq 1$	LC shape (a)
$N_{epochs}(-8 \leq p \leq 10) \geq 2$	SN peak luminosity
(two bands)	and color (a)
SN parameters	
$\sigma_{T_0} \leq 2$	LC sampling (b)
$\sigma_{x_1} \leq 1$	LC sampling (b)

One may notice that the SMoM metric is estimated by combining SNe Ia samples observed in the WFD (low-z) and DDF (high-z) surveys. It can not be used to check directly whether SNe Ia specifications (subsubsection 2.2.3) related to DDFs are fulfilled. But it has been shown that UDF scenarios with $z_{complete}^{UD}$ corresponding to SNe Ia requirements tend to maximize SMoM values (Gris et al. 2023).

4. Designing a cohesive DDF strategy

As shown in Section 2, measuring cosmological parameters (dark energy equation of state) with high accuracy with SNe Ia requires to observe (necessary condition) a large

sample of SNe Ia at higher redshifts ($z \geq 0.8$). This can be achieved with a high cadence of observation (≤ 2 night) and a large number of visits per observing night (more than 150 visits for a 2 night cadence) with a specific filter allocation defined by the z-depth to be reached (see Gris et al. (2023) for all the details). Nonetheless, this corresponds to a total number of visits (per season) quite costly in terms of budget: observing a SNe Ia sample up to a redshift completeness of ~ 0.75 leads to a fraction of DD visits of about 0.9% per season (Table 3). Since the DDF budget is limited to 5-7%, it is not realistic to design a uniform DD survey (leading to accurate cosmological measurements) where all the fields would be observed at the same cadence, with the same number of visits per observing night, and the same filter allocation, for ten years.

One possible solution is to design a DDF survey with two types of fields: ultra-deep fields leading to a high number of well-measured SNe Ia used to achieve accurate cosmological measurements; deep fields satisfying the 5-σ point source criteria from photo-z and WL. The depth (coadded 5-σ depth for photo-z/WL or $z_{\rm complete}$ for SNe Ia) is primarily driven by survey parameters such as the cadence and the number of visits per band and per observing night.

The method to design DESC cohesive DDF strategies proceeds in two steps. The first stage is to define a set of scenarios in a 4d parameter space: number of UD fields (and season of observation), number of visits per season of observation (for UDFs and DFs). Survey parameters such as cadence and season length of observation, filter allocation per observing night are to be defined in a second phase to build observing strategies from these scenarios. These parameters are chosen so that requirements from cosmological measurements are fulfilled (subsection 2.2).

The total number of DDF visits $N_{\rm v}^{\rm DDF}$ can be expressed as a function of eleven configuration parameters (see definitions in Table 5) characterizing a DDF scenario (in the following: f=field; s=season, v=visit):

$$N_{\rm v}^{\rm DDF} = N_{\rm v}^{\rm LSST} \times {\rm budget}^{\rm DD} \qquad (13)$$

$$N_{\rm v}^{\rm DDF} = N_{\rm f}^{\rm DF} \times N_{\rm s}^{\rm DF} \times N_{\rm v}^{\rm DF} + N_{\rm f}^{\rm UDF} \times N_{\rm s}^{\rm UDF} \times N_{\rm v}^{\rm UDF}$$
$$+ N_{\rm f}^{\rm UDF} \times (9 - N_{\rm s}^{\rm UDF}) \times N_{\rm v}^{\rm DF} + N_{\rm f}^{\rm Y1} \times N_{\rm v}^{\rm Y1} \qquad (14)$$

Combining Eqs (13) and (14) leads to:

$$A = [N_{\rm f}^{\rm UDF} \times (9 - N_{\rm s}^{\rm UDF}) + N_{\rm f}^{\rm DF} \times N_{\rm s}^{\rm DF}] \times N_{\rm v}^{\rm DF}$$
$$N_{\rm v}^{\rm UDF} = \frac{{\rm budget}^{\rm DD} \times N_{\rm v}^{\rm LSST} - N_{\rm f}^{\rm Y1} \times N_{\rm v}^{\rm Y1} - A}{N_{\rm f}^{\rm UDF} \times N_{\rm s}^{\rm UDF}} \qquad (15)$$

Photo-z/WL requirements for Y1 are different from the ones concerning Y2-Y10 (Table 2). This is why we chose to have a uniform DDF cadence in Y1 with observing strategy parameters (cadence of observation, season length, filter allocation) leading to surveys fulfilling photo-z/WL requirements. The observing strategy Y1 is thus the same for all the strategies proposed in this paper.

It is possible from Equation 15 to estimate the parameter space ($N_{\rm v}^{\rm DF}$, $N_{\rm v}^{\rm UDF}$) for a choice of ($N_{\rm f}^{\rm UDF}$, $N_{\rm s}^{\rm UDF}$) configurations if all other parameters are assigned the values of Table 5. Since SNe Ia requirements are related to the number of visits per observing night (subsubsection 2.2.3), we define a DDF strategy by the four parameters ($N_{\rm v}^{\rm UDF}$/obs.

night, $N_{\rm v}^{\rm DF}$, $N_{\rm f}^{\rm UDF}$, $N_{\rm s}^{\rm UDF}$). This requires to choose a cadence of observation ($\rm cad^{UDF}$) and season length ($\rm sl^{UDF}$) for UD fields. We have used $\rm cad^{UDF}=2$ nights and $\rm sl^{UDF}=180$ days in this paper.

Cohesive DDF strategies have to fulfill requirements from photo-z, WL and SNe Ia. We use a graphical method to define these strategies as described in the following. From Equation 15 we estimate the ($N_{\rm v}^{\rm UDF}$/obs. night, $N_{\rm v}^{\rm DF}$) parameter space (sets of lines) for three UD configurations ($N_{\rm f}^{\rm UDF}$, $N_{\rm s}^{\rm UDF}$)=[(2, 2),(2, 3),(2, 4)]. We superimpose to these results the parameter space corresponding to photo-z, WL and SNe Ia requirements (Section 2) which correspond to a set of vertical (photo-z+WL) and horizontal (SNe Ia) lines. DESC cohesive strategies parameters are defined by the intersection of these two parameter spaces. This graphical method (Figure 1) leads to the definition of 9 cohesive DDF strategies defined in Table 6. We observe that it is not possible to design scenarios fulfilling SNe Ia *and* photo-z/WL requirements with a DDF budget of 7%. Fulfilling all the requirements would require a DDF budget of $\sim 8.5\%$.

We have added two strategies on Figure 1. In the Deep Universal scenario all the DDFs are observed for ten years with the same cadence and the same depth (same number of visits per observing night). This scenario does not count any UD field. The SCOC_p2 scenario is designed from the SCOC phase 2 recommendations stipulating that the COSMOS field should have additionnal survey time to reach a depth corresponding to 10-year DDF within three years of LSST (subsection 2.1).

Completing the definition of the DESC cohesive DDF strategies requires to choose three additional parameters: season length, cadence of observation, and filter allocation (number of visits per band and per observing night). For UDFs, these parameters are coming from depth requirements related to the redshift completeness of the SNe Ia survey (subsection 2.2 and Table 5). For DFs, we have chosen a season length of 180 days (to maximize the number of observed SNe Ia) and a cadence of three days (median cadence observed in the simulations). The number of visits per band and per observing night (filter allocation) for the DFs is estimated from the total number of visits per season $N_{\rm v}^{\rm DF}$/season (Figure 1). $N_{\rm v}^{\rm DF}$/season is distributed among filters and observing nights in such a way that photo-z and WL requirements are fulfilled (subsubsection 2.2.1 and subsubsection 2.2.2). If this is not possible (which is the case for all the proposed scenarios except the ones optimal for photo-z/WL) the number of visits is split in such a way that the relative number of visits per band is equal to the one estimated from photo-z and WL requirements.

The LSST camera has 6 filters ($ugrizy$) and only five can be loaded in the filter exchange carousel. The current filter load strategy is to replace during daytime one of the z or y by the u band at the start of dark time, when the lunar phase is lower than 20%. The process is reversed when the lunar phase is above 20%. We have performed a study using SNe Ia to assess the impact of the swap $z \leftrightarrow u$ or $y \longleftrightarrow u$ on two metrics ($z_{\rm complete}$ and $N_{\rm SN}^{z \leq z_{\rm complete}}$). The results are detailed in Appendix A . The conclusion is that the minimal loss is observed for the $y \leftrightarrow u$ swap. This can be explained by the fact that the number of visits in the y band is lower than the number of visits in the z band. The decrease of the light curve signal-to-noise ratio due to the swap is lower if y and u bands are exchanged. Following the

Table 5: List of parameters defining DDF scenarios. Constraints are taken from the SCOC phase 2 recommendations, photo-z/WL calibration constraints, and SNe Ia cosmological requirements.

parameter	definition	constraint	source
$\text{budget}^{\text{DD}}$ N_v^{LSST}	DD budget total number of LSST visits	5-7% 2.1 million	SCOC phase 2 recommendations Survey simulation
N_f^{Y1} N_v^{Y1}	Number of fields observed in season 1 Number of visits per field in season 1	5 1187	SCOC phase 2 recommendations photo-z/WL req.
N_f^{UDF} N_s^{UDF} N_v^{UDF} $N_s^{\text{UDF,DF}}$	Number of UD fields Number of seasons for UD fields Number of visits (per season) per UD field Number of seasons of UD fields = Deep fields	2 2-4 14580-26820 9-N_s^{UDF}	SNe Ia req. SNe Ia req. SNe Ia req. SCOC phase 2 recommendations
N_f^{DF} N_s^{DF} N_v^{DF}	Number of Deep fields Number of seasons for Deep fields Number of visits (per season) per Deep field	5-N_f^{UDF} 9 1525	SCOC phase 2 recommendations SCOC phase 2 recommendations photo-z,WL req.
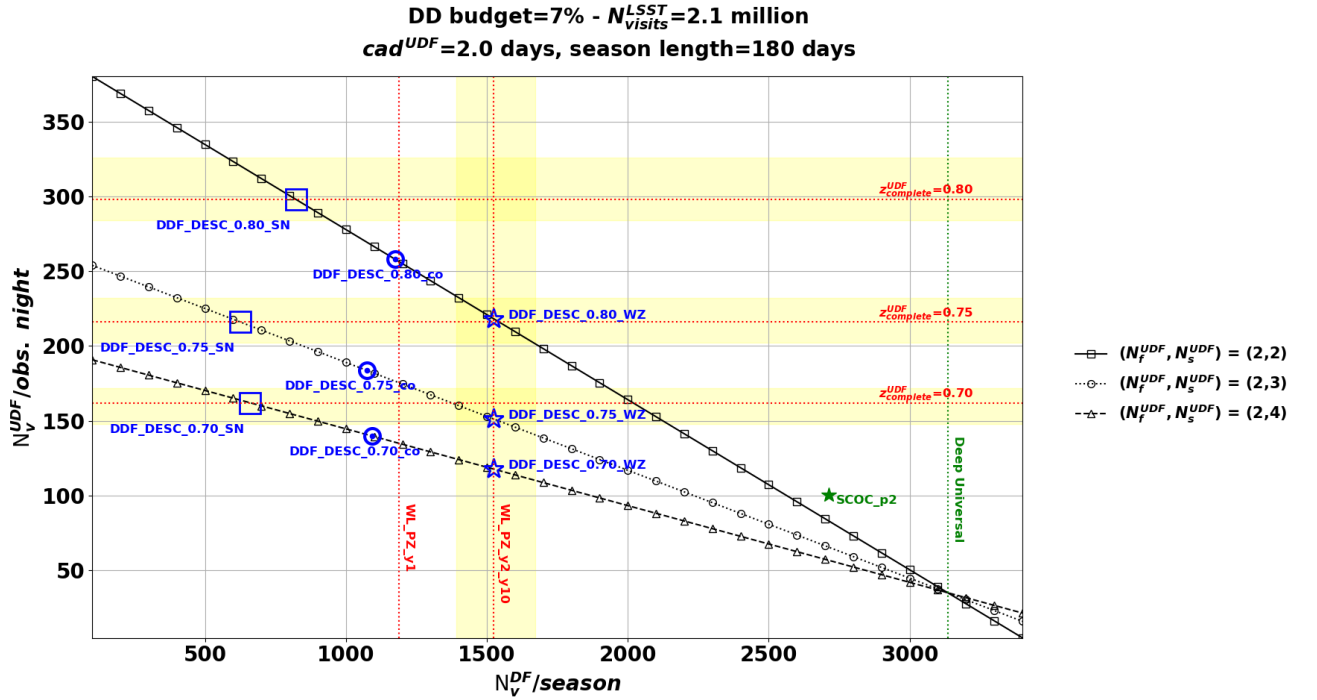
Fig. 1: Graphical estimation of the parameters of DESC cohesive DDF strategies in the (N_v^{UDF}/observing night, N_v^{DF}/season) parameter space. Black lines correspond to three configurations (N_f^{UDF},N_s^{UDF}) for a budget of 7%, a number of visits of 2.1 million, a cadence of observation of 2 days and a season length of 180 days for UDFs. The (N_v^{UDF}/observing night, N_v^{DDF}/season) parameter space corresponding to photo-z+WL (calibration) requirements (red dotted vertical lines) and SNe Ia cosmological constraints (red dotted horizontal lines) is used to define the strategies (intersection points with the lines corresponding to the three (N_f^{UDF},N_s^{UDF}) configurations. On this plot are also reported the results corresponding to the SCOC phase 2 recommendations (SCOC_p2) and to a universal survey. Yellow areas around photo-z+WL and SNe Ia requirements correspond to Δm_5^b=±0.05 and $\Delta z_{\text{complete}}$=±0.01, respectively. Markers correspond to strategies optimal for SNe Ia (squares), fulfilling photo-z/WL requirements (stars), or corresponding to compromises between photo-z/WL and SNe Ia constraints (circles).

Table 6: List of DESC cohesive scenarios. Requirements are fulfilled if $\Delta N_{visits} \geq 0$ (photo-z/WL) or $\Delta z^{\mathrm{UD}}_{\mathrm{complete}} \geq 0$ (SNe Ia).

| Strategy | Requirements | | $(\mathrm{N}_{\mathrm{f}}^{\mathrm{UDF}}, \mathrm{N}_{\mathrm{s}}^{\mathrm{UDF}})$ | Note |
	$\Delta z^{\mathrm{UD}}_{\mathrm{complete}}$	ΔN_{visits}		
DDF_DESC_0.80_SN		-701	(2,2)	optimal
DDF_DESC_0.75_SN	0	-899	(2,3)	for
DDF_DESC_0.70_SN		-865	(2,4)	SN
DDF_DESC_0.80_WZ			(2,2)	optimal
DDF_DESC_0.75_WZ	-0.05	0	(2,3)	for
DDF_DESC_0.70_WZ			(2,4)	PZ/WL
DDF_DESC_0.80_co		-351	(2,2)	compromise
DDF_DESC_0.75_co	-0.03	-450	(2,3)	between
DDF_DESC_0.70_co		-433	(2,4)	PZ/WL and SN

Fig. 2: Photo-z metric Δm_5 for the proposed strategies, for each DDF and each band. Photo-z requirements are fulfilled if $\Delta m_5 \geq 0$. The dashed line corresponds to $\Delta m_5 = 0$.

conclusion of this study we have swapped the y and u bands when the lunar phase is low in the design of the proposed strategies. The total number of u (y) visits is distributed among the nights with a Moon phase lower (higher) than 20%.

The observing strategy parameters for the proposed DESC cohesive scenarios are summarized on Figures B.1-B.2. Exposure times are given in Tables B.2-B.1. The coadded 5-σ depth and the total number of visits per field-/band/season are given in Table B.3. As expected, the number of visits per observing night increases with the
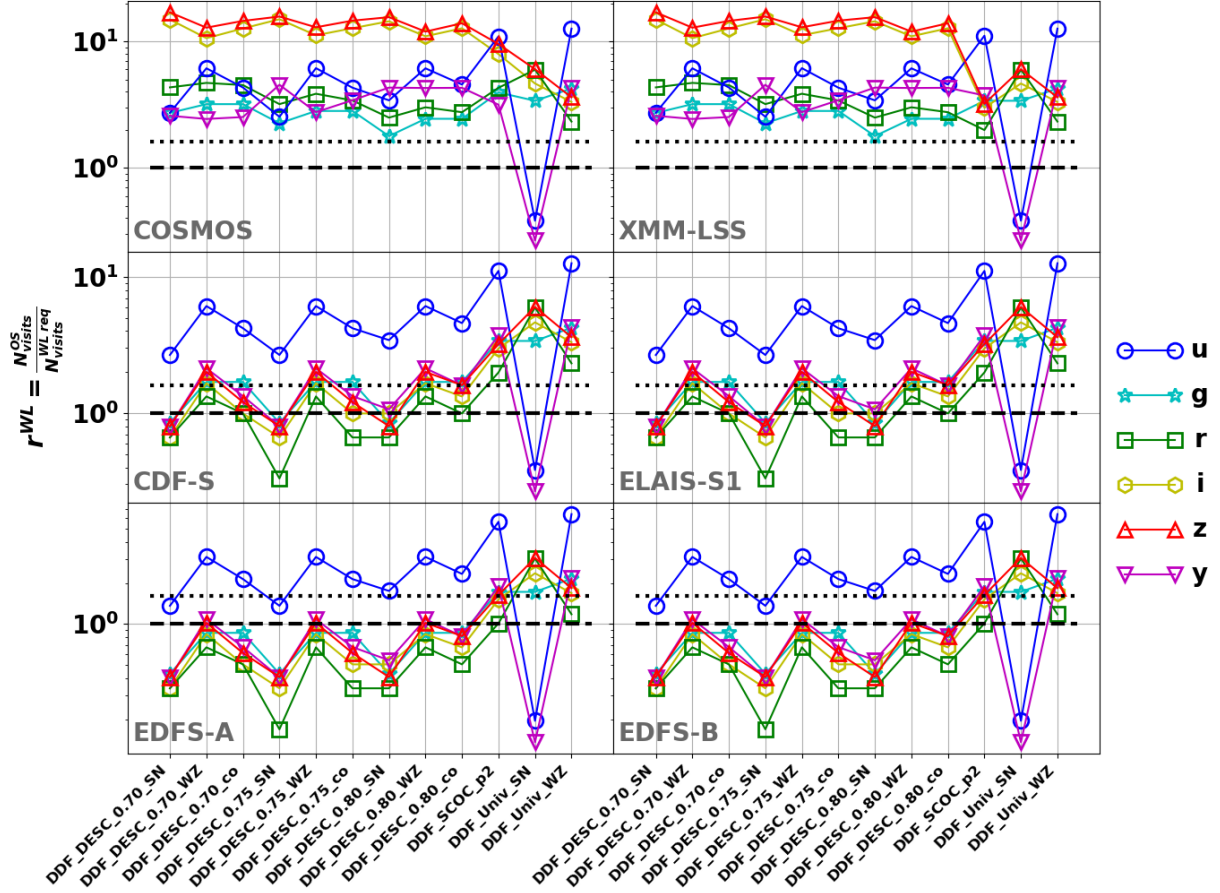
Fig. 3: WL metric $r^{WL} = \frac{N_{visits}^{OS}}{N_{visits}^{WL\ req}}$ for the proposed strategies and for each field/band. The dashed (dotted) line correspond to r^{WL}=1 (1.6). WL requirements are fulfilled if $r^{WL} \geq 1$.

depth of observation (z_{complete}) and higher values (about 300 visits that is 2.5 hours of observing time) are reached for $z_{\mathrm{complete}} \sim 0.80$ in the DDF_DESC_0.80_SN scenario. As expected, a large fraction of the DDF budget is exhausted after few seasons for strategies with two UDFs (i.e. DDF_DESC_* scenarios - Figure B.3).

5. Assessment of the proposed DESC cohesive DDF strategies

5.1. Simulation of the proposed strategies

Assessing the DESC cohesive strategies (Section 4) using the metrics defined in Section 3 requires to have simulations of the proposed scenarios. We have performed these simulations using the parameters defined in Figure B.1 and Figure B.2. We have used median observing conditions per season for the only observing parameter considered, the 5-σ depth parameter. We are aware of the imprecise nature of these simulations. But they can be used to provide some insight about the relative performance of the proposed scenarios. As will be stresses below, the preliminary findings obtained in this study need to be checked with more accurate simulations using the LSST scheduler.

5.2. Photo-z metric

The photo-z metric defined in Sec. 3, $\Delta m_5 = m_5^{OS} - m_5^{PZ\ req}$, is estimated using the above-described simulations. Photo-z requirements are fulfilled if $\Delta m_5 \geq 0$.

Results for season 1 (Table C.1) show that two bands, u and g, do not meet photo-z requirements for the COS-MOS field, with $\Delta m_5 \sim$ -0.08 and -0.11, respectively. These differences correspond to a one observing night variation in the survey. Most of the bands for EDFS-a and EDFS-b do not fulfill photo-z requirements. This can be explained by the fact that the total number of visits for these two fields is twice lower (SCOC phase 2 recommendations). Δm_5 is positive for r and i bands because the number of visits for season 1 is driven by WL requirements (Tab. 2).

Results for seasons 2-10 are given on Figure 2. UDFs tend to meet photo-z requirements for all the bands but the u one. The larger number of visits in $grizy$ bands for UDFs explains this result. As expected u-band photo-z requirements are fulfilled for scenarios corresponding to an optimization of photo-z and WL criteria. A variation of $\Delta m_5 \sim$ -0.5 is observed for strategies built to meet SNe Ia requirements. This u-band result for UDFs is to be extended to all the bands for CDF-S and ELAIS-S1 where lower values of $\Delta m_5 \sim$ -0.5 are reached for optimal SN strategies. Lower Δm_5 values of $\sim$-1 mag are reached by z band measurements for EDFS-a and EDFS-b. As for
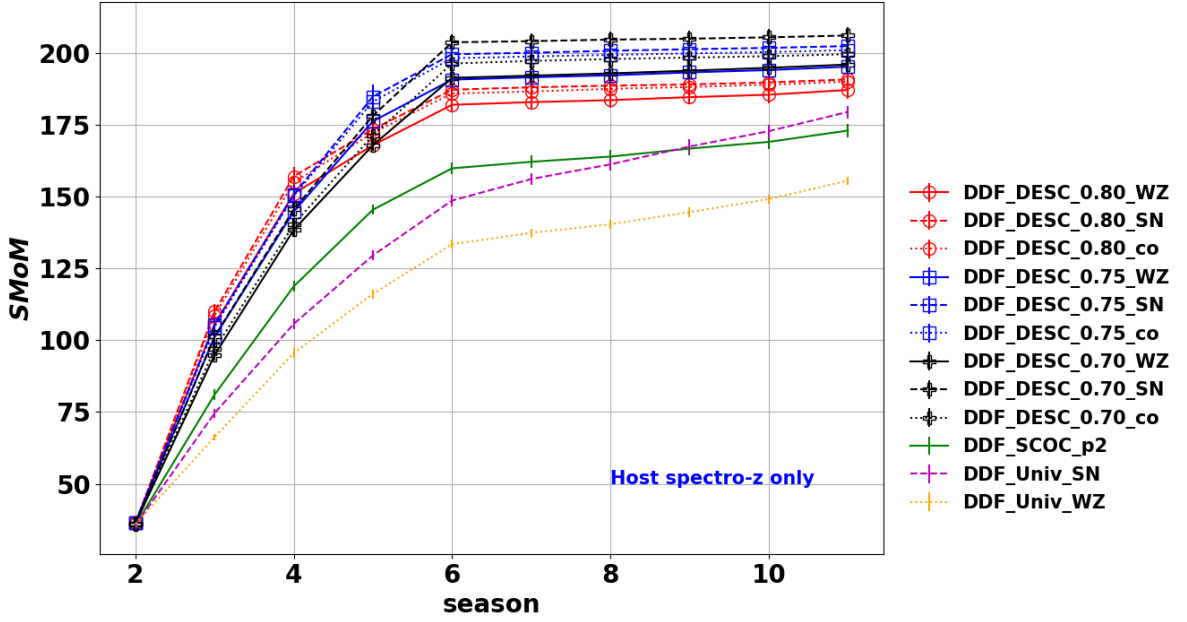
Fig. 4: SNe Ia metric SMoM as a function of the season for all the strategies designed in this paper. A prior on Ω_m is added to Equation 10 ($\sigma_{\Omega_m} = 0.0073$ Aghanim et al. (2020)) to achieve these results. The observed sample is composed exclusively of SNe Ia with spectroscopic host galaxy redshift.

season 1, these results are to be explained by the lower depth of these fields. One may observe that the scenario DDF_Univ_SN is far from meeting the minimum requirements for u and y bands.

5.3. WL metric

The WL metric defined in Section 3, $r^{WL} = \frac{N_{visits}^{OS}}{N_{visits}^{WL\ req}}$, is estimated using the above-described simulations. WL requirements are fulfilled if $r^{WL} \geq 1$.

Season 1 results (Tab. C.2) show that WL requirements are met for all fields except for ECDFS-a and ECDFS-b in the southern region. The number of visits in r,i,z,y for season 1 is driven by WL requirements (Tab. 2). r^{WL} is thus close to one for these bands and for all fields but EDFS-a and EDFS-b. For these two fields the number of visits is a factor of 2 lower compared to the other DDFs (SCOC phase 2 recommendations) and the ratio is close to ~ 0.5. For this season the requirement $r^{WL} \gtrsim 16$ (subsubsection 2.2.2) is fullfiled for all the fields but EDFS-a and EDFS-b and only for u and g bands.

WL requirements are exceeded for UDFs observations during seasons 2 to 10 for all the strategies but DDF_Univ_SN. r^{WL} lies in the range [3-10] with higher values corresponding to z and y bands. Results for CDF-S and ELAIS-S1 are much more mitigated. Except the u-band, WL requirements are fulfilled for all scenarios but the ones corresponding to strategies optimal for SN. The situation is worse for southernmost fields EDFS-a and EDFS-b where WL requirements are not met (except the u-band) for all strategies with UDFs.

5.4. SNe Ia metric

The SMoM metric is estimated from a Hubble diagram cosmological fit and requires to have a sample of SNe Ia in the redshift range [0.01,1.1]. We thus generate a SNe Ia sample observed in a WFD survey using the baseline_v3.0_10yrs simulation (see Appendix C). This sample is then combined to each of the proposed DDF strategies to estimate SMoM values.

We assume that the SNe Ia used to estimate SMoM have host galaxy redshifts measured from spectroscopic observations. We (conservatively) consider two spectroscopic resources contemporaneous with LSST to provide vital spectra and host redshifts, PFS/Subaru (Tamura et al. 2016) and 4MOST/TiDES (de Jong et al. (2019); Swann et al. (2019)). The PFS/Subaru spectroscopic follow-up survey is designed to observe two of the northernmost LSST DDFs, COSMOS and XMM-LSS. About 20,000 host galaxy redshifts up to $z \sim 0.8$ will be measured after ten years. The 4MOST/TiDES survey is dedicated to the spectroscopic follow-up of extragalactic optical transients. About 50,000 host galaxy redshifts up to $z \sim 1$ will be collected for 5 years. This corresponds both to the WFD and the DD fields. The fraction of SNe Ia expected to have secure redshift measurements is taken from Mandelbaum et al. (2019) (Figure 1, right plot).

SMoM values are displayed on Figure 4. As expected an increase of SMoM is observed up to season 6 ($\sim$7,000 SNe Ia from the WFD survey are added each season) when 4MOST/TiDES is expected to end its 5-year survey. After season 6, only SNe Ia observed in DDFs are added to the SNe Ia sample used to estimate SMoM. A saturation of SMoM values is observed in season 6 for all the strate-

Table 7: SMoM values (ascending order) after a 10-season survey. The standard deviation corresponding to SMoM distribution resulting from the fit of 50 random surveys is also quoted.

Observing Strategy	SMoM
DDF_Univ_WZ	155 ± 1
DDF_SCOC_p2	173 ± 2
DDF_Univ_SN	179 ± 2
DDF_DESC_0.80_WZ	187 ± 3
DDF_DESC_0.80_co	190 ± 2
DDF_DESC_0.80_SN	191 ± 3
DDF_DESC_0.75_WZ	195 ± 2
DDF_DESC_0.70_WZ	196 ± 1
DDF_DESC_0.70_co	199 ± 3
DDF_DESC_0.75_co	201 ± 2
DDF_DESC_0.75_SN	202 ± 4
DDF_DESC_0.70_SN	206 ± 3

Table 8: Mean Δm_5^b values for field/band that do not fulfill photo-z requirements for the DDF_DESC_*_co strategies.

Field	band	Δm_5^b
COSMOS	u	-0.26
XMM-LSS	u	-0.16
CDF-S	r	-0.05
	u	-0.10
	y	-0.23
	z	-0.26

gies having two UDFs. Final SMoM values (full survey) are given in Table 7.

Measuring cosmological parameters (w_0, w_a) with high accuracy (i.e. maximizing SMoM) requires to observe (necessary condition) a large sample of well-measured SNe Ia at higher redshifts (Gris et al. 2023). Scenarios with UDFs lead (by design) to samples with ~ 1000, ~ 1500, ~ 1800 SNe Ia with $z \geq 0.8$ for DDF_DESC_0.80*, DDF_DESC_0.75*, DDF_DESC_0.70* observing strategies, respectively (Figure D.1). Furthermore, a large fraction of SNe Ia in these samples (65-80%, 40-60%, 20-40%, respectively) lead to accurate distance measurements $(\sigma_\mu \leq \sigma_{int})$.

We have estimated SMoM for surveys composed of spectroscopic and photometric ($\mathcal{O}(10,000)$ per year for ten years) host galaxy redshifts. These surveys lead to higher SMoM values (as expected) but also to biased fits. Studying the origin of the biases requires additional work (beyond the scope of this paper). At this stage the SNe Ia metric proposed in this paper, SMoM, should only be used with surveys with spectroscopic host galaxy redshifts.

5.5. Combining metric results

A quick analysis of the metric results (Figs 2-4) tend to show that the strategies leading to highest SMoM values do not all fulfill photo-z and WL requirements. It may be interested to study in more details these strategies both to quantify to which extent the requirements are not met and propose adjustments of the strategies designed in this paper.

The list of strategies that do not fulfill photo-z or WL requirements is given on Figure 5 along with photo-z and WL metric values. The fields EDFS-a and EDFS-b are not included in this results (photo-z and WL requirements are difficult to meet for these fields which are observed at a depth twice lower than the other fields). WL requirements are fulfilled by DDF_DESC_0.80_co and DDF_DESC_0.70_co. For DDF_DESC_0.75_co requirements are not met for the r-band and two fields (ELAIS-S1 and CDF-S). This could be solved by adding one r-band visit per observing night. It would correspond to a (very modest) increase of the DD budget of $\sim 0.05\%$.
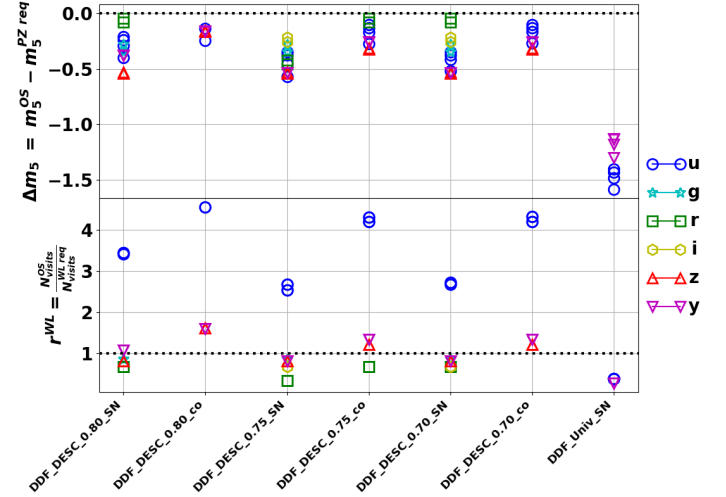

Fig. 5: Photo-z (top) and WL (bottom) metric values for field/band/strategy that do not fulfill photo-z or WL requirements. The dotted lines correspond to $\Delta m_5^b = 0$ (photo-z requirement, top) and $r^{WL} = 1$ (WL requirement, bottom). Southernmost fields (EDFS-a and EDFS-b) were not included.

Observations used for photo-z calibration (reference catalogs listed in subsubsection 2.2.1) overlap with COSMOS, XMM-LSS and CDF-S. Mean Δm_5^b values for these three fields are given in Table 8. A lower depth with respect to reference observations would not be optimal for photo-z calibration (a fraction of COSMOS2020 galaxy sample of 89% and 74% would be used for Δm_5^b -0.2 and -0.5 mag, respectively) but the final impact has to be estimated using more realistic simulations of the strategies proposed in this paper.

In summary, the most promising strategies are the ones optimal for photo-z/WL requirements (DESC_DDF*_WZ). These surveys lead to highest SMoM values whilst fulfilling photo-z/WL requirements. Observing strategies corresponding to a compromise between the constraints from photo-z, WL and SNe Ia (DESC_DDF*_co) lead to high SMoM, fulfill WL requirements, but are close (i.e. showing the highest $\Delta m_5^b < 0$) to meet photo-z constraints. Further studies are needed to quantify the impact of these strategies on photo-z calibration. Strategies optimal for SNe Ia do not

fulfill photo-z and WL requirements. Fulfilling photo-z/WL constraints for these strategies requires to increase the DDF budget to 8.5%.

6. Conclusion

Cosmological measurements with LSST rely heavily on the DDFs for photometric redshift training, weak gravitational lensing, and particularly to provide a deep sample of high-redshift SNe Ia. In this paper we have proposed a method to design a set of DESC cohesive DDF strategies fulfilling both constraints from cosmological measurements (calibration requirements for photo-z and WL, precision cosmology for SNe Ia) and recommendations from the SCOC. We have simulated these strategies and we have defined a set of metrics (for each science case) to evaluate their performance.

Our conclusion is that it seems possible to design DDF surveys meeting the specifications. The most promising results are obtained with deep rolling surveys composed of deep fields (cadence of observation: ~ 3 nights; 30-40 visits per observing night) and of ultradeep fields (cadence of observation: $\lesssim 2$ nights; 80-100 visits per observing night for 3 to 4 seasons; same cadence as deep fields thereafter). These surveys (like DESC_DDF_*_WZ) lead to the most accurate cosmological measurements for time domain science whilst fulfilling requirements for static science for extragalactic deep fields.

The method used in this paper to design such cohesive strategies is based on the depth required to perform accurate calibration of primary systematic uncertainties (photo-z, WL) and precise cosmological measurements (SNe Ia). It could be used to design other large surveys.

All the strategies proposed in this paper correspond to a DDF budget of $\sim 7\%$, the maximal budget recommended by the SCOC. We have shown that it was not possible in this budget to design cohesive strategies fulfilling all requirements (photo-z/WL *and* SNe Ia). A DDF budget of $\sim 8.5\%$ is required to design observing strategies satisfying all the cosmological requirements. This 1.5% DDF budget increase would lead to an increase of up to 5% of SMoM values.

SNe Ia results have highlighted the necessity to observe a large sample of SNe Ia in the WFD survey leading to accurate distance measurements ($\sigma_\mu \lesssim \sigma_{int}$). It was also shown that the filter load strategy consisting of swapping u and y bands according to the Moon phase leads to higher number of SNe Ia at higher redshifts. It should be the (default) filter load strategy used in LSST.

These results were achieved with a relatively basic simulation as far as observing parameters (skybrightness, clouds, dithering) are concerned. A validation with realistic simulations using the LSST scheduler is required. These simulations would help to estimate realistic metric values and may lead to a tuning of the survey parameters of the cohesive DDF strategies proposed in this paper.

Author contributions are listed below.
Ph. Gris: initiated, set up and coordinated the analysis as DESC Observing Strategy/Survey Coordination Working Group co-convener; conceptualization, methodology (sections 3-5) software, analysis (metrics), writing (original draft; review & editing); formal analysis of the SNe Ia parts;
H. Awan: initiated, coordinated, and contributed to the paper as the DESC Observing Strategy Working Group co-convener with Ph. Gris, building on years of engagement as an active OSWG member;
M. Becker: developed the weak lensing DDF requirements and provided extensive feedback on the text of the document.
H. Lin: developed photo-z DDF requirements and provided related text.

Appendix A: Impact of the filter load strategy on SNe Ia metrics

To study the impact of the filter load strategy on SNe Ia metrics we generate a set of strategies where the filter u is exchanged with one of the other filters ($rizy$) with varying Moon phases. For each of these strategies we simulate and fit SNe Ia light curves to extract SNe Ia parameters used to estimate the redshift completeness z_{complete} and the number of well-sampled SNe Ia, N_{SN}.

Observing strategies are generated with a regular cadence (two nights) and a number of visits per observing night equal to 10/2/9/50/81/28 with a single visit 5σ-depth equal to 23.48/24.26/23.87/23.46/22.76/22.02 for $u/g/r/i/y/z$ bands, respectively. The lunar phase value to exchange the u band ranges from 0% to 40%. We generate one season with a length of 180 days.
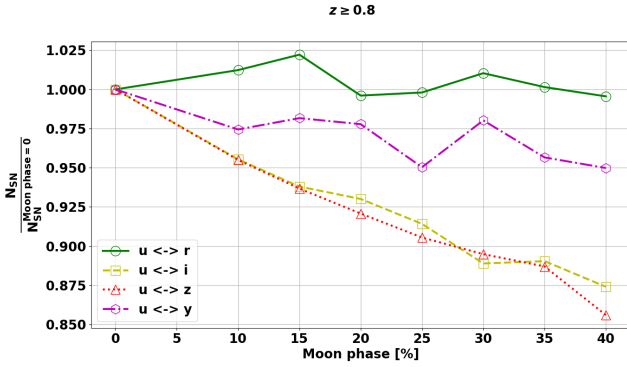

Fig. A.1: The number of well-sampled SNe Ia with $z \geq 0.8$, N_{SN}, normalized to the configuration where the Moon phase is equal to 0 (i.e. no swap), as a function of the Moon phase threshold corresponding to the swap of the u filter.
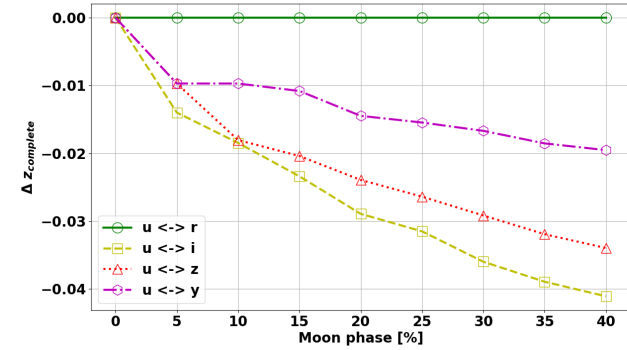
- z random in [0.01,1.1]
- (x_1,c)=(-2.0,0.2) to estimate z_{complete}
- (x_1,c) randomly distributed using the G10 intrinsic scatter model (Scolnic & Kessler (2016)) to estimate N_{SN}.

The following tight selection criteria are applied:

- only light-curve points with S/N ≥ 1 are considered;
- at least 4 epochs before the maximum of luminosity and 10 epochs after the maximum luminosity are required;
- at least one point with a phase lower than -10 and one point with a phase higher than 20 are required; and
- $\sigma_c \leq 0.04$ is required to ensure accurate distance measurement.

By definition, for this study, a well-sampled (or well-observed) SN Ia fulfills these criteria. The redshift limit is defined as the maximum redshift of supernovae passing these selection criteria. The redshift of a complete sample, z_{complete}, is estimated from the redshift limit distribution, $z_{\text{lim,faint}}^{\text{SN}}$, of a simulated set of intrinsically faint supernovae (i.e. with $(x_1, c) = (-2.0, 0.2)$) with T_0 values spanning over the season duration of a set of observations. z_{complete} is defined as the 95th percentile of the $z_{\text{lim,faint}}^{\text{SN}}$ cumulative distribution.

The number of well-sampled SNe Ia , N_{SN}, and the z_{complete} variation, both normalized to the configuration where the Moon phase is equal to 0, as a function of the Moon phase are given in Figure A.1 and Figure A.2 for the following filter load configuration: $u \leftrightarrow r, u \leftrightarrow i, u \leftrightarrow z, u \leftrightarrow y$. As expected the swap $u \leftrightarrow r$ has a limited effect since the SNe Ia flux is mainly collected with the izy bands in the considered redshift range. The lowest impact is observed for the $u \leftrightarrow y$ configuration.

Fig. A.2: z_{complete} variation, normalized to the configuration where the Moon phase is equal to 0 (i.e. no swap), as a function of the Moon phase threshold corresponding to the swap of the u filter.

We use these strategies to simulate and fit SNe Ia light curves using SALT3 with:

- T_0 random in [MJD$_{\text{min}}$,MJD$_{\text{max}}$] where MJD$_{\text{min}}$ and MJD$_{\text{max}}$ are the min and max MJD of the season, respectively.

Appendix B: DESC cohesive DDF strategies

A definition of the observing strategies proposed in this paper is provided in Figure B.1 and Figure B.2. The number of visits (per observing night) as a function of the season is given for each of the fields considered. The filter allocation (i.e. the number of visits per band and per observing night) and the cadence of observation (per season) are also mentioned. A summary of exposure times is given in Table B.1 (season 1) and Table B.2 (seasons 2-10). The coadded 5-σ depth and the total number of visits per field-/band/season are given on Table B.3.

Table B.1: Exposure times for season 1.

	nightly [sec]	season [h]
Moon phase > 20%	480	28.3
Moon phase ≤ 20%	930	24.3

Table B.2: Exposure times (in hours) for seasons 2-10.

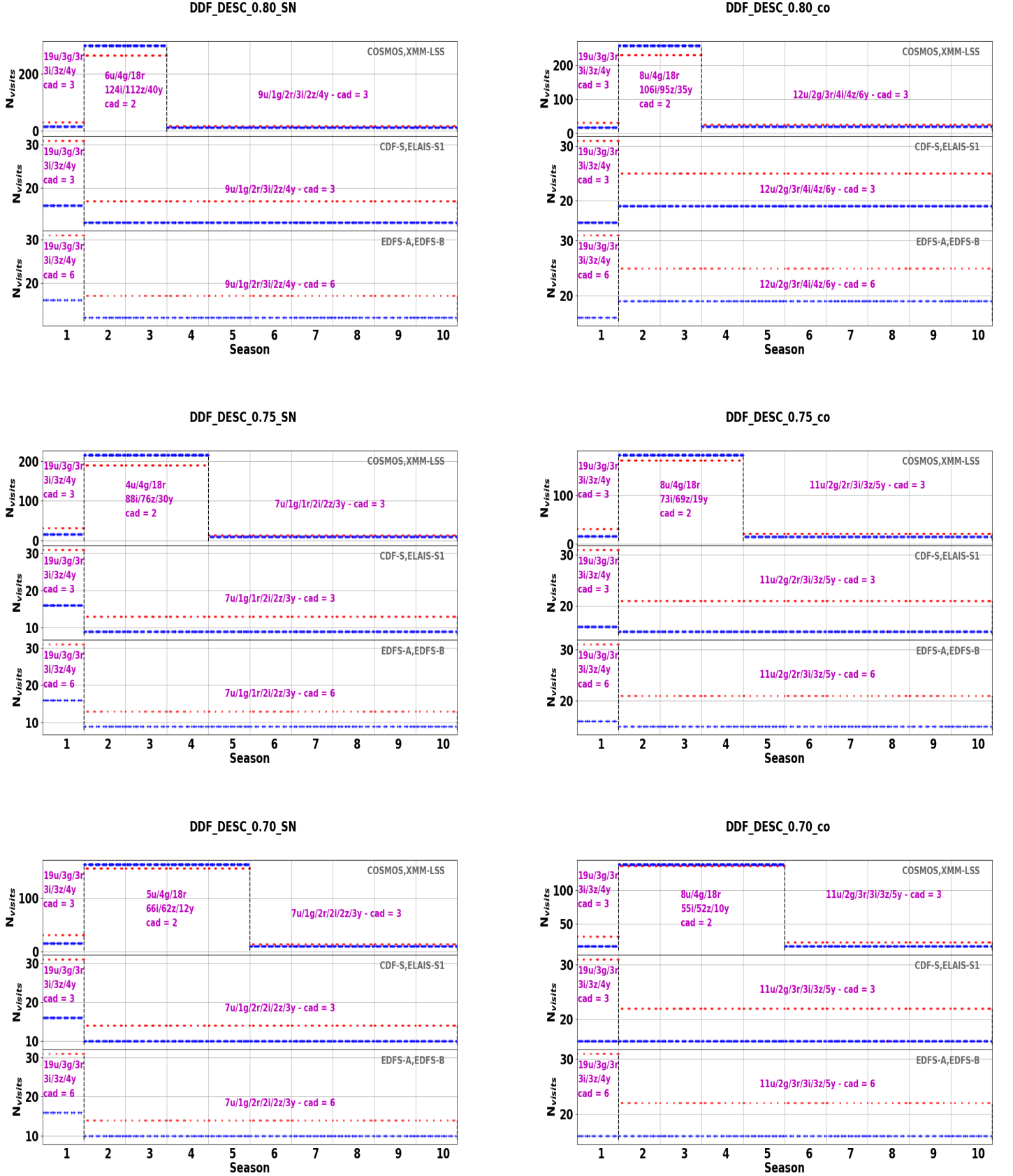| Strategy	nightly		survey
	UDF	DF	
DDF_DESC_0.80_WZ	1.8	0.2	1195.2
DDF_DESC_0.80_SN	2.5	0.1	1153.9
DDF_DESC_0.80_co	2.2	0.2	1191.9
DDF_DESC_0.75_WZ	1.3	0.2	1213.9
DDF_DESC_0.75_SN	1.8	0.1	1150.7
DDF_DESC_0.75_co	1.5	0.1	1152.2
DDF_DESC_0.70_WZ	1.0	0.2	1215.5
DDF_DESC_0.70_SN	1.4	0.1	1181.7
DDF_DESC_0.70_co	1.2	0.1	1175.8
DDF_SCOC_p2	0.8	0.3	1212.0
DDF_Univ_SN	0.4	0.4	1193.4
DDF_Univ_WZ	0.4	0.4	1196.0

Fig. B.1: Number of visits as a function of the season for COSMOS, XMM-LSS, CDF-S, ELAIS-S1, EDFS-a, EDFS-b fields for several considered DESC cohesive DDF strategies. Red points correspond to nights with a lunar phase lower than 20%. Blue crosses correspond to nights with a lunar phase higher than 20%. The filter allocation (per observing night) and the cadence of observation (per season) are specified for each season (magenta).

Fig. B.2: Number of visits as a function of the season for COSMOS,XMM-LSS, CDF-S, ELAIS-S1, EDFS-a, EDFS-b fields for the remaining DESC cohesive DDF strategies. Red points correspond to nights with a lunar phase lower than 20%. Blue crosses correspond to nights with a lunar phase higher than 20%. The filter allocation (per observing night) and the cadence of observation (per season) are specified for each season (magenta).
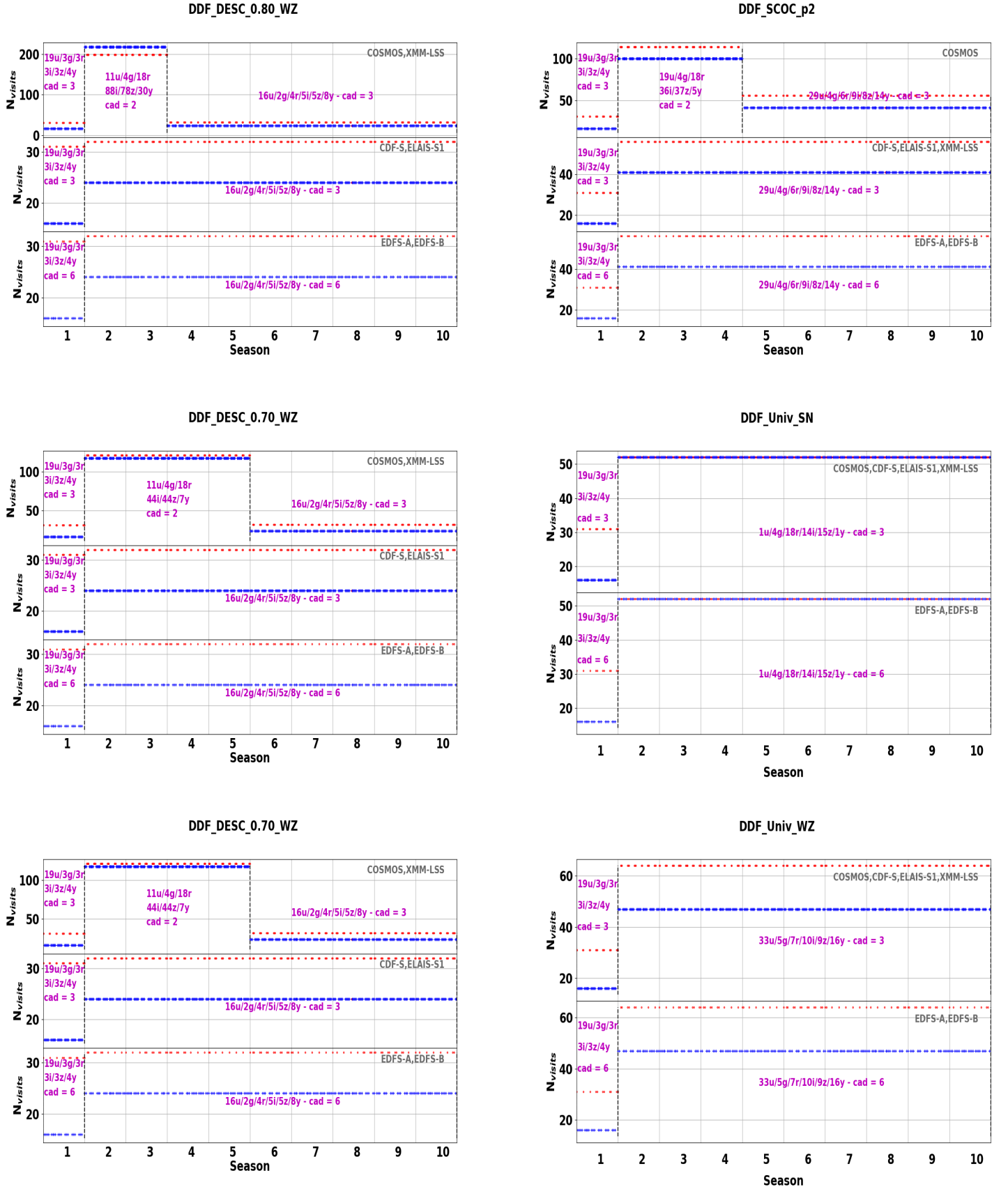
Table B.3: Coadded 5-σ depth and total number of visits N_v per band.

Strategy	Field	season	m_5 u/g/r/i/z/y	N_v u/g/r/i/z/y
DDF_DESC_0.80_WZ	UDF	1	26.6/27.0/26.7/26.3/25.5/24.7	342/183/183/183/183/172
		2-10	27.7/28.3/28.6/28.9/28.1/26.8	2643/1582/4984/18151/16331/6158
	DF	1	27.0/27.4/26.9/26.5/25.7/25.0	342/183/183/183/183/172
		2-10	27.9/28.2/28.1/27.9/27.2/26.5	2640/1098/2196/2745/2745/3072
DDF_DESC_0.80_SN	UDF	1	26.6/27.0/26.7/26.3/25.5/24.7	342/183/183/183/183/172
		2-10	27.4/28.2/28.5/29.0/28.2/26.8	1476/1155/4130/23849/21238/6204
	DF	1	27.0/27.4/26.9/26.5/25.7/25.0	342/183/183/183/183/172
		2-10	27.6/27.8/27.8/27.6/26.7/26.1	1485/549/1098/1647/1098/1536
DDF_DESC_0.80_co	UDF	1	26.6/27.0/26.7/26.3/25.5/24.7	342/183/183/183/183/172
		2-10	27.6/28.3/28.5/29.0/28.2/26.8	1968/1582/4557/21000/18998/6181
	DF	1	27.0/27.4/26.9/26.5/25.7/25.0	342/183/183/183/183/172
		2-10	27.7/28.2/28.0/27.8/27.0/26.3	1980/1098/1647/2196/2196/2304
DDF_DESC_0.75_WZ	UDF	1	26.6/27.0/26.7/26.3/25.5/24.7	342/183/183/183/183/172
		2-10	27.7/28.4/28.7/28.9/28.1/26.5	2651/1824/6378/18483/17664/3968
	DF	1	27.0/27.4/26.9/26.5/25.7/25.0	342/183/183/183/183/172
		2-10	27.9/28.2/28.1/27.9/27.2/26.5	2640/1098/2196/2745/2745/3072
DDF_DESC_0.75_SN	UDF	1	26.6/27.0/26.7/26.3/25.5/24.7	342/183/183/183/183/172
		2-10	27.2/28.3/28.6/29.0/28.3/26.8	1094/1458/5280/24756/21480/6528
	DF	1	27.0/27.4/26.9/26.5/25.7/25.0	342/183/183/183/183/172
		2-10	27.5/27.8/27.4/27.4/26.7/26.0	1155/549/549/1098/1098/1152
DDF_DESC_0.75_co	UDF	1	26.6/27.0/26.7/26.3/25.5/24.7	342/183/183/183/183/172
		2-10	27.5/28.4/28.6/28.9/28.2/26.6	1858/1824/5646/21027/19935/4928
	DF	1	27.0/27.4/26.9/26.5/25.7/25.0	342/183/183/183/183/172
		2-10	27.7/28.2/27.8/27.6/26.9/26.2	1815/1098/1098/1647/1647/1920
DDF_DESC_0.70_WZ	UDF	1	26.6/27.0/26.7/26.3/25.5/24.7	342/183/183/183/183/172
		2-10	27.7/28.4/28.8/28.8/28.1/26.4	2644/2066/7772/17541/17541/3504
	DF	1	27.0/27.4/26.9/26.5/25.7/25.0	342/183/183/183/183/172
		2-10	27.9/28.2/28.1/27.9/27.2/26.5	2640/1098/2196/2745/2745/3072
DDF_DESC_0.70_SN	UDF	1	26.6/27.0/26.7/26.3/25.5/24.7	342/183/183/183/183/172
		2-10	27.3/28.4/28.7/29.0/28.2/26.5	1177/1761/7162/24634/23178/3714
	DF	1	27.0/27.4/26.9/26.5/25.7/25.0	342/183/183/183/183/172
		2-10	27.5/27.8/27.8/27.4/26.7/26.0	1155/549/1098/1098/1098/1152
DDF_DESC_0.70_co	UDF	1	26.6/27.0/26.7/26.3/25.5/24.7	342/183/183/183/183/172
		2-10	27.5/28.4/28.8/28.9/28.2/26.4	1865/2066/7467/20935/19843/3630
	DF	1	27.0/27.4/26.9/26.5/25.7/25.0	342/183/183/183/183/172
		2-10	27.7/28.2/28.0/27.6/26.9/26.2	1815/1098/1647/1647/1647/1920
DDF_SCOC_p2	UDF	1	26.6/27.0/26.7/26.3/25.5/24.7	342/183/183/183/183/172
		2-10	28.0/28.5/28.7/28.7/28.0/26.5	4729/2556/7110/13122/13029/4544
	DF	1	27.0/27.4/26.9/26.5/25.7/25.0	342/183/183/183/183/172
		2-10	28.2/28.6/28.3/28.2/27.4/26.8	4785/2196/3294/4941/4392/5376
DDF_Univ_SN	UDF	1	26.6/27.0/26.7/26.3/25.5/24.7	342/183/183/183/183/172
		2-10	26.2/28.4/28.8/28.3/27.7/25.2	165/2196/9882/7686/8235/384
	DF	1	27.0/27.4/26.9/26.5/25.7/25.0	342/183/183/183/183/172
		2-10	26.4/28.6/28.9/28.4/27.8/25.4	165/2196/9882/7686/8235/384
DDF_Univ_WZ	UDF	1	26.6/27.0/26.7/26.3/25.5/24.7	342/183/183/183/183/172
		2-10	28.1/28.5/28.3/28.1/27.4/26.7	5445/2745/3843/5490/4941/6144
	DF	1	27.0/27.4/26.9/26.5/25.7/25.0	342/183/183/183/183/172
		2-10	28.3/28.7/28.4/28.3/27.5/26.9	5445/2745/3843/5490/4941/6144

Appendix C: Simulation results

The proposed DDF strategies have been simulated using simplified observing conditions (median 5-σ depth per field/season) and metrics have been processed using these strategies as input.

The cumulative DD budget as a function of the season is given on Figure B.3. As expected (by design) strategies with two UDFs use a large part of the budget in a few seasons (more than 80% in 4 seasons for DDF_DESC_0.70* surveys).

Results of the PZ metrics are given on Table C.1 for the first year of the survey. PZ requirements are fulfilled for all the fields/band but EDFS-a andEDFS-b (differences for u and z bands for COSMOS are due to a one night difference in the simulations w.r.t. the requirements). Differences observed for EDFS-a and EDFS-b are explained by the fact that these fields are not as deep as other DDFs (SCOC phase 2 recommendations).

Results of the WL metrics are given on Table C.2 for the first year of the survey. WL requirements are met for all fields/bands.

We have performed a simulation of the WFD survey using the LSST simulation baseline_v3.0_10yrs. We have simulated a sample of SNe Ia corresponding to 10 times the number of expected SNe Ia (we use the rate from Hounsell et al. (2018)) in the full redshift range [0.01,0.7]. We use the G10 intrinsic scatter model (Scolnic & Kessler (2016)) where (x_1,c) distributions are described by asymmetric gaussian distributions with three parameters. We choose random T_0 values spanning over the season duration of a group of observations.

SNe Ia fulfilling the selection criteria defined in Table 4 make-up the sample of well-measured SNe Ia used for cos-
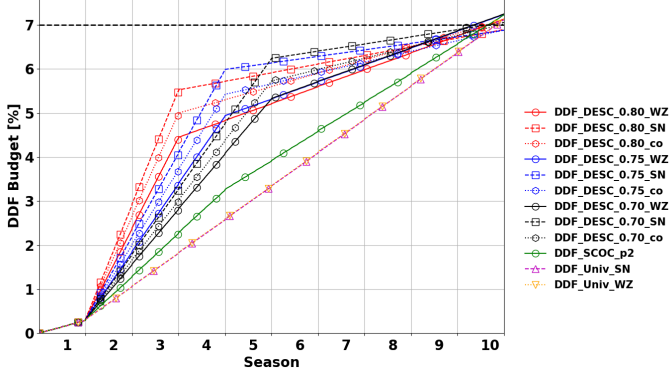
Fig. B.3: Cumulative DDF budget as a function of the season. A large fraction of the budget is consumed in a few seasons for strategies with two UDFs (i.e. DDF_DESC* scenarios).

Table C.1: $\Delta m_5 = m_5^{OS} - m_5^{PZ\ req}$ for year 1. photo-z requirements are fulfilled if $\Delta m_5 \geq 0$.

season	band	$\Delta m_5 = m_5^{OS} - m_5^{PZ\ req}$
COSMOS/ XMM-LSS	u	-0.08/0.18
	g	0.01/0.50
	r	0.49/0.85
	i	0.52/0.83
	z	-0.11/0.38
	y	0.04/0.43
CDF-S/ ELAIS-S1	u	0.30/0.21
	g	0.36/0.28
	r	0.67/0.66
	i	0.72/0.85
	z	0.09/0.35
	y	0.29/0.40
EDFS-a/ EDFS-b	u	-0.10/-0.07
	g	-0.06/-0.08
	r	0.23/0.30
	i	0.19/0.36
	z	-0.30/-0.24
	y	-0.13/-0.16

Table C.2: $\frac{N_{visits}^{OS}}{N_{visits}^{WL\ req}}$ for year 1. ELAIS-S1, XMM-LSS, and CDF-S fields have similar results to COSMOS, and EDFS-b to EDFS-a. WL requirements are fulfilled if $\frac{N_{visits}^{OS}}{N_{visits}^{WL\ req}} \geq 1$.

season	band	$\frac{N_{visits}^{OS}}{N_{visits}^{WL\ req}}$
COSMOS/ EDFS-a	u	7.12/4.35
	g	2.54/1.29
	r	0.99/0.51
	i	0.99/0.51
	z	1.20/0.61
	y	1.08/0.50

mology measurements. About $\sim 900{,}000$ SNe Ia are expected to be observed after ten years (Figure C.1) with a rate between 70,000 and 120,000 SNe Ia per year. About 10-15% of the observed SNe Ia lead to accurate distance measurements ($\sigma_\mu \leq \sigma_{int}$).
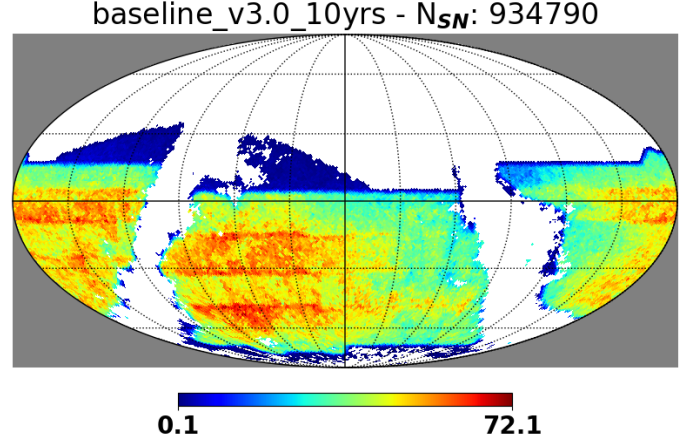
Fig. C.1: Number of SNe Ia after ten years for the WFD survey of baseline_v3.0_10yrs.

Appendix D: Metric results

The number of well-measured SNe Ia with $z \geq 0.8$ used to estimate SMoM (Figure 4) as a function of the season is given on Figure D.1 for the strategies proposed in this paper. Scenarios with UDFs lead clearly to a higher number of SNe Ia at higher redshifts. Highest numbers are reached with DDF_DESC_0.70* strategies. This is expected, as UDFs, by design, provide a large part (more than 80% for DDF_DESC_0.70_co) of the SNe Ia sample for $z \geq 0.8$.
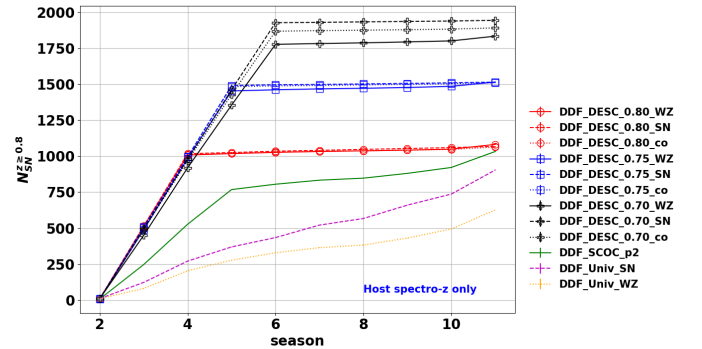

Fig. D.1: Number of well-sampled SNe Ia with $z \geq 0.8$.

SMoM values displayed in Figure 4 are estimated using a random distribution ($z \in [0.01, 0.4]$) for the redshifts of the SNe Ia observed in the WFD sample. This choice reflects the way TiDES will observe the sky ((Swann et al. 2019)) but it leads to samples with a low number of SNe Ia at low redshifts ($z \lesssim 0.1-0.2$). We have processed the SMoM metric on samples maximizing the number of low z SNe Ia of the WFD survey. An increase of SMoM is of $\sim$12-13% is observed.

References

Abate, A. 2012, Large Synoptic Survey Telescope: Dark Energy Science Collaboration

Abell, L. S. C. P. A., Allison, J., Anderson, S. F., et al. 2009, LSST Science Book, Version 2.0

Aghanim, N., Akrami, Y., Ashdown, M., et al. 2020, Astronomy & Astrophysics, 641, A6

Albrecht, A., Bernstein, G., Cahn, R., et al. 2006, Report of the Dark Energy Task Force

Almoubayyed, H., Mandelbaum, R., Awan, H., et al. 2020, Monthly Notices of the Royal Astronomical Society, 499, 1140

Alves, C. S., Peiris, H. V., Lochner, M., McEwen, J. D., & Kessler, R. 2023, The Astrophysical Journal Supplement Series, 265, 43

Awan, H., Gawiser, E., Kurczynski, P., et al. 2016, The Astrophysical Journal, 829, 50

Barbary, K., Barclay, T., Biswas, R., et al. 2016, Astrophysics Source Code Library, record ascl:1611.017

Bernstein, G. M. & Armstrong, R. 2014, MNRAS, 438, 1880

Bernstein, G. M., Armstrong, R., Krawiec, C., & March, M. C. 2016, MNRAS, 459, 4467

Betoule, M., Kessler, R., Guy, J., et al. 2014, Astronomy & Astrophysics, 568, A22

Bianco, F. B., Ivezić, Ž., Jones, R. L., et al. 2021, 258, 1

Brout, D., Scolnic, D., Popovic, B., et al. 2022, The Pantheon+ Analysis: Cosmological Constraints

Buchs, R., Davis, C., Gruen, D., et al. 2019, Monthly Notices of the Royal Astronomical Society, 489, 820–841

Chevallier, M. & Polarski, D. 2001, International Journal of Modern Physics D, 10, 213–223

de Jong, R., Agertz, O., Berbel, A. A., et al. 2019, 4MOST: Project overview and information for the First Call for Proposals

et al, J. D. H. 2007, Computing in Science & Engineering, 9, 5

Gris, P., Regnault, N., Awan, H., et al. 2023, The Astrophysical Journal Supplement Series, 264, 22

Guy, J., Sullivan, M., Conley, A., et al. 2010, Astronomy & Astrophysics, 523, A7

Hartley, W. G., Choi, A., Amon, A., et al. 2021, Monthly Notices of the Royal Astronomical Society, 509, 3547

Hoekstra, H., Herbonnet, R., Muzzin, A., et al. 2015, MNRAS, 449, 685

Hoekstra, H., Viola, M., & Herbonnet, R. 2017, MNRAS, 468, 3295

Hounsell, R., Scolnic, D., Foley, R. J., et al. 2018, The Astrophysical Journal, 867, 23

Huff, E. & Mandelbaum, R. 2017, Metacalibration: Direct Self-Calibration of Biases in Shear Measurement

Huterer, D., Takada, M., Bernstein, G., & Jain, B. 2006, Monthly Notices of the Royal Astronomical Society, 366, 101

Ivezić, v., Kahn, S. M., Tyson, J. A., et al. 2019, The Astrophysical Journal, 873, 111

Jarvis, M. J., Bonfield, D. G., Bruce, V. A., et al. 2012, Monthly Notices of the Royal Astronomical Society, 428, 1281

Kenworthy, W. D., Jones, D. O., Dai, M., et al. 2021, The Astrophysical Journal, 923, 265

Le Fèvre, O., Cassata, P., Cucciati, O., et al. 2013, A&A, 559, A14

Linder, E. V. 2003, Physical Review Letters, 90

Lochner, M., Scolnic, D., Almoubayyed, H., et al. 2021a, The Impact of Observing Strategy on Cosmological Constraints with LSST

Lochner, M., Scolnic, D., Almoubayyed, H., et al. 2021b, The LSST Dark Energy Collaboration Cadence Note

Lochner, M., Scolnic, D. M., Awan, H., et al. 2018, Optimizing the LSST Observing Strategy for Dark Energy Science: DESC Recommendations for the Wide-Fast-Deep Survey

MacCrann, N., Becker, M. R., McCullough, J., et al. 2022, MNRAS, 509, 3371

Mandelbaum, R. 2018, Annual Review of Astronomy and Astrophysics, 56, 393

Mandelbaum, R., Blazek, J., Chisari, N. E., et al. 2019, Wide-field Multi-object Spectroscopy to Enhance Dark Energy Science from LSST

Mauduit, J.-C., Lacy, M., Farrah, D., et al. 2012, Publications of the Astronomical Society of the Pacific, 124, 714

McCracken, H. J., Milvang-Jensen, B., Dunlop, J., et al. 2012, A&A, 544, A156

McKinney, W. 2011, in pandas: a Foundational Python Library for Data Analysis and Statistics

Myles, J., Alarcon, A., Amon, A., et al. 2021, MNRAS, 505, 4249

Price-Whelan, A. M., Sipőcz, B. M., Günther, H. M., et al. 2018, The Astronomical Journal, 156, 123

Scolnic, D. & Kessler, R. 2016, The Astrophysical Journal, 822, L35

Scolnic, D. M., Lochner, M., Gris, P., et al. 2018, Optimizing the LSST Observing Strategy for Dark Energy Science: DESC Recommendations for the Deep Drilling Fields and other Special Programs

Sheldon, E. S. & Huff, E. M. 2017, The Astrophysical Journal, 841, 24

Stanford, S. A., Masters, D., Darvish, B., et al. 2021, ApJS, 256, 9

Swann, E., Sullivan, M., Carrick, J., et al. 2019, 4MOST Consortium Survey 10: The Time-Domain Extragalactic Survey (TiDES)

Sánchez, C. & Bernstein, G. M. 2018, Monthly Notices of the Royal Astronomical Society, 483, 2801–2813

Tamura, N., Takato, N., Shimono, A., et al. 2016, Ground-based and Airborne Instrumentation for Astronomy VI

The Rubin Observatory Survey Cadence Optimization Committee. 2022, Survey Cadence Optimization Committe's Phase 2 Recommendations

van der Walt, S., Colbert, S. C., & Varoquaux, G. 2011, Computing in Science & Engineering, 13, 22

Virtanen, P., Gommers, R., Oliphant, T. E., et al. 2020, Nature Methods, 17, 261

Weaver, J. R., Kauffmann, O. B., Ilbert, O., et al. 2022, The Astrophysical Journal Supplement Series, 258, 11

Zhang, Z., Sheldon, E. S., & Becker, M. R. 2023, The Open Journal of Astrophysics, 6